Atomic Structure of Interface States in Silicon Heterojunction Solar Cells

B. M. George,[1] J. Behrends,[2] A. Schnegg,[1,*] T. F. Schulze,[1] M. Fehr,[1] L. Korte,[1] B. Rech,[1] K. Lips,[1] M. Rohrmüller,[3] E. Rauls,[3] W. G. Schmidt,[3] and U. Gerstmann[3,†]

[1]*Institut für Silizium-Photovoltaik, Helmholtz-Zentrum Berlin für Materialien und Energie, Kekuléstraße 5, D-12489 Berlin, Germany*
[2]*Fachbereich Physik, Freie Universität Berlin, Arnimallee 14, D-14195 Berlin, Germany*
[3]*Lehrstuhl für Theoretische Physik, Universität Paderborn, Warburger Straße 100, D-33098 Paderborn, Germany*

(Received 30 October 2012; published 26 March 2013)

Combining orientation dependent electrically detected magnetic resonance and g tensor calculations based on density functional theory we assign microscopic structures to paramagnetic states involved in spin-dependent recombination at the interface of hydrogenated amorphous silicon crystalline silicon (a-Si:H/c-Si) heterojunction solar cells. We find that (i) the interface exhibits microscopic roughness, (ii) the electronic structure of the interface defects is mainly determined by c-Si, (iii) we identify the microscopic origin of the conduction band tail state in the a-Si:H layer, and (iv) present a detailed recombination mechanism.

DOI: 10.1103/PhysRevLett.110.136803 PACS numbers: 73.20.−r, 72.20.Jv, 73.40.−c, 88.40.jj

Semiconductor interfaces play an important role in solid state physics and are crucial for the function of countless devices [1]. Since structure sizes in microelectronics shrink in order to realize higher integration densities or lower processing costs (e.g., for solar cells), surfaces or interfaces gain in importance [2]. Heterostructures [3] and organic semiconductor devices [4] are based completely on the functionality of interfaces. The structural discontinuity present at interfaces often gives rise to electronic states that may lead to trapping or recombination of charge carriers, thereby interfering with device function. Controlling the impact of surface or interface-derived electronic states is, thus, a prime goal in modern semiconductor processing. To this end, ultrathin semiconducting or dielectric layers such as amorphous silicon (-oxide or -nitride), zinc selenide or aluminum oxide are commonly employed. These materials form heterojunctions which significantly differ in band lineup, space charge layers, and specific defects [5–7]. Despite their technological importance, the electronic structure of many of these interfaces remains under dispute.

A paradigm heterojunction, employed, e.g., in state-of-the-art high-efficiency solar cells, is formed at the a-Si:H/c-Si interface [8]. Here, similar to other crystalline-amorphous boundaries, the microscopic structure-function relationship is still in dispute. Open questions concern (i) the morphology of the interface region under nm-thin a-Si:H layers [9,10], (ii) the electronic structure of the heterointerface [11,12] and (iii) of its native interface defects [13,14], and (iv) the prevailing charge carrier transport and recombination mechanisms at the p/n junction [15,16]. The tool of choice for structural characterization of paramagnetic interface states and studying spin-dependent transport processes in real devices is provided by electrically detected magnetic resonance (EDMR) [17]. In particular g tensors derived from magnetic resonance are routinely used as fingerprints for paramagnetic states at Si interfaces [18–22]. The amount of information that can be extracted from the measured g tensors is substantially extended by advanced computational methods that allow for their reliable numerical simulation [23–25]. So far, however, such an analysis has been restricted to localized defects. Extended states such as band tail states have not been tackled in this context yet.

In this Letter, we combine continuous wave (cw) EDMR spectroscopy on a-Si:H/c-Si solar cells with density functional theory (DFT) g tensor calculations of interface states, in order to explore their electronic properties. Anisotropies of two different dangling bonds at the [111]-oriented interface are exploited to locate the observed spin dependent transport process in the multilayer solar cell. By a DFT analysis of the magnetic Berry phases [26] we assign atomic structures even to extended states in the a-Si:H tissue close to the interface. Combining these pieces of information, electron hole recombination, via conduction band tail states and paramagnetic dangling bond defects, is identified as dominating interface mechanism at low temperatures.

Miniature a-Si:H/c-Si heterojunction solar cells were prepared on [111]-oriented boron-doped (p)c-Si wafers with 1–3 Ω cm resistivity with a mirror-polished front side and a rough backside resulting from KOH etching. A hetero-emitter of 8 nm (n)a-Si:H was deposited by PECVD at $T = 210°C$. The front contact was realized by 80 nm of transparent conductive ZnO:Al and evaporation of a 200 nm thick aluminum grid. After a separate HF dip, the backside was covered with aluminum to provide the back contact. A similar solar cell design has been shown to yield an efficiency of 17.4% [27].

The solar cells were measured in a BRUKER E580 X-band EPR spectrometer equipped for electrical detection [28]. The sample was kept at $T = 18$ K. White light was applied through a window in the cryostat whereby the

 © 2013 American Physical Society

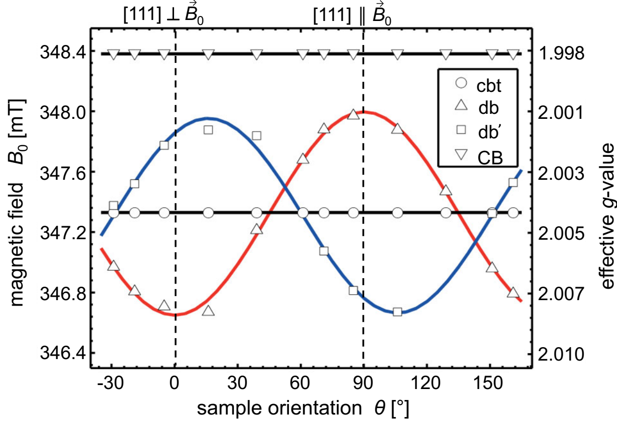

FIG. 1 (color online). cw-EDMR of a-Si:H/c-Si solar cells as a function of $\vec{B}_0$ and θ, the orientation of $[1\bar{2}1]$ to $\vec{B}_0$ taken under white light illumination at 18 K. Symbols: Peak positions of 1 Gaussian (*cbt*) and 3 Lorentzian (*db*, *db*′, CB) lines. Solid lines: Fit (black) to *cbt* [$g = 2.004(1)$] and CB [$g = 1.998(1)$]. Fit to *db* (red) and *db*′ (blue) with the same g values [$g_\parallel = 2.001(1)$, $g_\perp = 2.008(1)$], but with different orientation [*db*′ shifted by $\phi = 106(2)°$].

device shows solar cell behavior exhibiting $V_{OC} = 0.73$ V and $I_{SC} \approx -0.1$ mA/cm^2. cw-EDMR spectra were taken under forward bias +0.64 V within an angular range of about 200°, varying the angle θ between $\vec{B}_0$ and the $[1\bar{2}1]$ direction in the sample. All spectra were fitted simultaneously with a model consisting of three Lorentzian and one Gaussian lines (see Supplemental Material [29]). In Fig. 1, the fitted peak positions of each deconvoluted EDMR spectrum are plotted against the angle θ. Two lines with fixed and two lines with varying spectral positions are clearly distinguishable. Isotropic lines contributing to the EDMR spectra are found at $g_{cbt} = 2.004(1)$ and $g_{CB} = 1.998(1)$. Due to their orientation dependence, we assign the resonances *db* and *db*′ to defect states at the interface. The peak positions of *db* were fitted with a g tensor with principal values $g_{11} = g_{22} = g_\perp = 2.008(1)$ and $g_{33} = g_\parallel = 2.001(1)$. $g_\parallel$ and $g_\perp$ are oriented parallel and perpendicular to the [111] direction of the crystal, respectively. *db*′ was fitted with a g tensor exhibiting the same principal values, but with a different orientation. Its $g_\parallel$-axis encloses an angle of $\phi = 106(2)°$ with the surface normal of the crystal (cf. Table I). The close similarity to the well-known P_b center at the Si/SiO$_2$ interface [19,30] may be surprising, but similar results have been reported by EPR [20]. The backside of the wafer can be excluded as an origin, since the detected signal intensity depends on the applied bias voltage, which is not expected for the highly defective back interface with a pinned Fermi level. The detection of two defects at the interface with different orientations indicates a microscopic roughness and is in agreement with findings reported by Angermann *et al.* [31] after HF dip of a [111] Si crystal surface.

TABLE I. Experimental (EDMR) and theoretical g tensors (DFT): localized defects (*db*, *db*′) calculated via linear magnetic response (GIPAW)[23]; extended (*cbt*) and delocalized states (CB) via orbital magnetization, $\Delta g_{\mu\nu} = \frac{\partial M_\mu^{\rm orb}}{\partial S_\nu}$ [26].

	Model	$g_{11} = g_\perp$	$g_{22} = g_\perp$	$g_{33} = g_\parallel$	ϕ [°]
EDMR	*db*	2.008(1)	2.008(1)	2.001(1)	0(2)
DFT		2.0082	2.0093	2.0015	2
EDMR	*db*′	2.008(1)	2.008(1)	2.001(1)	106(2)
DFT		2.0079	2.0092	2.0019	110
EDMR	*cbt*	2.004(1)	2.004(1)	2.004(1)	···
DFT		2.0046	2.0046	2.0038	···
EDMR	CB	1.998(1)	1.998(1)	1.998(1)	···
DFT		1.9990	1.9990	1.9990	···

The g tensors of the paramagnetic states contain detailed information about their electronic structure and the (de) localization of the half-filled orbitals into the Si network [25]. In order to fully extract this information and to gain insight into transport related defects on the atomic scale [21], the EDMR data have to be complemented with *ab initio* DFT calculations on a-Si:H/c-Si model structures. For such structures, we calculated the elements of the electronic g tensor from first principles, using the gauge-including projector augmented plane wave (GI-PAW) approach [23] as implemented in the QUANTUM-ESPRESSO package [32]. We used norm-conserving pseudopotentials with a 30 Ry energy cut-off. Electron exchange and correlation effects were taken into account using the gradient-corrected functional of Perdew, Burke, and Erzerhof (PBE) functional in its spin-polarized form [33]. The deviation of the g tensor from the free-electron value g_e is given by spin-orbit coupling as mediated by the spin currents $\vec{j}(\vec{r})$ induced by the external magnetic field [23,24], whereby the explicit treatment of an external magnetic field $\vec{B}_0$ has to be done in a gauge-invariant way. We modeled the a-Si:H/c-Si interface in slabs with periodic boundary conditions. In order to allow for a full description of the anisotropies of a single spin, the supercell contains only a single a-Si:H/c-Si interface. The interaction of the periodic images of the slabs are quenched by introducing a 10 Å vacuum layer into the supercell. Numerical convergence is reached using eight layers of crystalline Si (the bottom layer was saturated with H atoms) within a 8×4 translational symmetry that was covered with a 1 nm-thick a-Si:H containing 84 Si and 17 H, close to the 17% H/Si ratio usually found in thin a-Si:H heteroemitters [34].

For such an ensemble of altogether 217 atoms, molecular dynamics (MD) simulations were performed by heating up the structure to 500 K. In some cases, this resulted in dangling bonds that evolved in the amorphous part. We obtained a large variation of anisotropic g tensors with average g values between 2.0038 and 2.0054, in full agreement with recent results for a-Si:H bulk material [25]. In the majority of cases, broken bonds were formed directly at

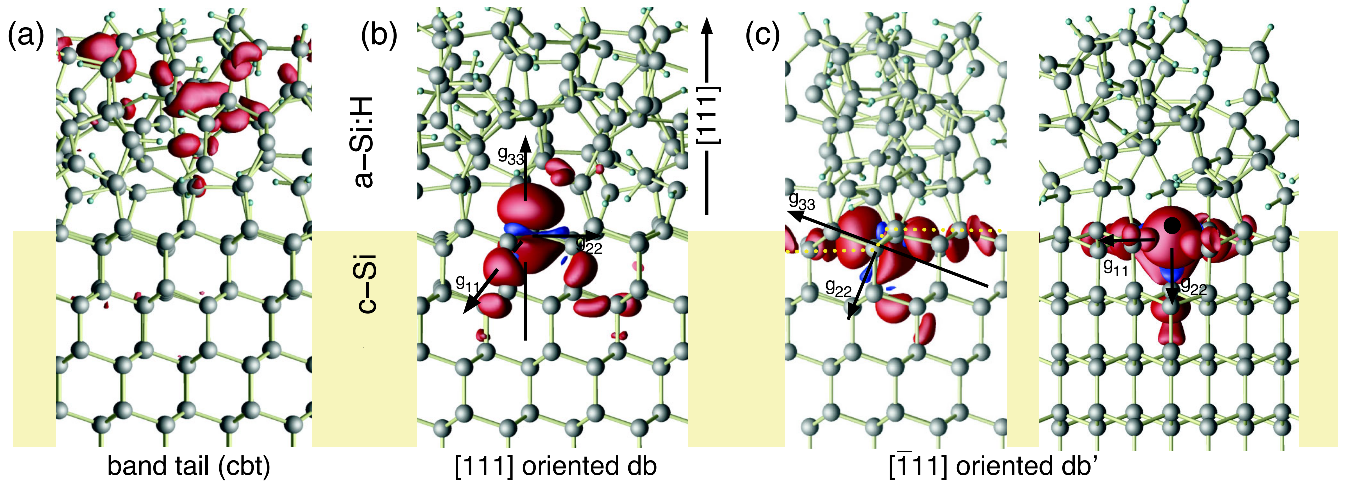

FIG. 2 (color online). Calculated magnetization density (giving rise to the EDMR pattern) for the recombination-active structures (red: positive, blue: negative): (a) prototype conduction band tail, (b) P_b-like [111]-oriented dangling bond (*db*) at the heterojunction, and (c) a tilted, 110° off-axis oriented dangling bond (db') at a microstep of monatomic height (dotted line). Large spheres: Si, Small spheres: H.

the interface. Besides [111]-oriented defects at flat regions of the interface [cf. Fig. 2(b)], dangling bonds aligned 110° from the interface normal were also formed at monoatomic steps [Fig. 2(c)]. In both cases, the magnetization density, i.e., the density of the unpaired electron, is localized within a tripod built up by three crystalline Si zigzag chains. This trigonal symmetry is also reflected in the g tensor and explains the close similarities of the *db* signal with the P_b center at the Si/SiO_2 [111] interface. Note that the tilted defect (db' signal) resembles the so-called P_{b0} center at the Si/SiO_2 [001] interface, but in contrast to the latter (one zigzag chain within the interface [21]), it shows an inverted behavior with two legs of the tripod along the interface.

Returning to the discussion of the isotropic signals, a value close to $g_{cbt} = 2.004$ is known for conduction band tail states in bulk *a*-Si:H [35,36]. Indeed, our DFT calculations exhibit a conduction band tail state, with a nearly isotropic $g \approx 2.004$ already for the ultrathin 1 nm-thick *a*-Si:H layer in the heterostructure [cf. Fig. 2(a)]. For larger, e.g., 8 nm-thick layers, an even more isotropic g tensor can be expected. The corresponding structure was modeled with an additional (excess) electron trapped at the bottom of the conduction band. For this system with quasidegenerate, partially filled states, perturbation theory is not applicable. Instead, we have derived the g tensor via a Berry phase formula for the orbital magnetization where the spin-orbit coupling enters explicitly the Hamiltonian of the self-consistent cycle [26]. We use the same approach to calculate the g tensor for the strongly delocalized conduction band (CB) electrons in crystalline silicon. Assuming the CB electron to be trapped at the six equivalent CB valleys around $(0, 0, 0.85)2\pi/a$, we calculated an isotropic g value of 1.9990 in excellent agreement with the experimental value of 1.9995 [37]. Within the experimental uncertainty, a value of 1.998(1) observed for the CB line in the heterostructure is in accordance with the evaluated signature of conduction electrons in *c*-Si bulk material.

Table I summarizes experimentally and theoretically determined g tensors including their orientation ϕ with respect to the [111] interface normal, showing an overall excellent agreement. The remaining questions concern the identification of the underlying transport processes leading to the detected EDMR resonances. Information may be obtained from the position, the sign, and the temperature dependence of the cw-EDMR lines. We found that the signals *cbt*, *db*, and db' are current decreasing, a typical property of recombination processes. Their line intensities peak around 18 K, while CB peaks at lower temperatures. In conclusion, we exclude the CB signal from this recombination process. Common temperature dependence and current quenching property of the three remaining signals *cbt*, *db* and db' confirm a common transport mechanism dominated by spin-dependent recombination. Since the sum of their EDMR-line integrals is not constant, they may, however, also be involved in additional, recombination-competing processes. Such processes may include hopping transport via band tail states in bulk *a*-Si:H leading to EDMR resonances close to $g = 2.0046$–48, but with opposite sign compared to recombination processes [36,38–40]. Contributions of ZnO:Al states to the orientation independent EDMR signals are excluded, since EDMR active states in ZnO:Al exhibit different g values [28].

In Fig. 3 (left) the calculated densities of states (DOS) for the model structures *cbt*, *db*, and db' are displayed (cf. Fig. 2). The energetic peak positions are consistent with the character of the EDMR signals and, thus, with a spin-dependent recombination process (cf. the qualitative band diagram sketched in Fig. 3, right): After tunneling into the *a*-Si:H layer [16], excess electrons from the *c*-Si wafer will be captured in conduction band tail states

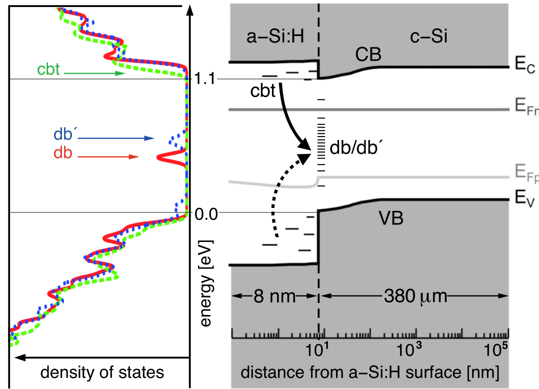

FIG. 3 (color online). Left: Density of states (DOS) calculated for the interface structures depicted in Fig. 2 (*cbt*, *db*, *db′*). The DFT gap was corrected by a 0.5 eV scissor shift [42] for the delocalized (CB-like) states. Right: Qualitative band diagram of the $(n)a$-Si:H/$(p)c$-Si heterointerface with applied forward bias. E_C (E_V), E_{Fn} (E_{Fp}) mark conduction (valence) band edges and electron (hole) quasi-Fermi levels, respectively. E_{Fn}, E_{Fp} coincide at the electric contacts (not included). Recombination process: Under illumination an electron is trapped in *a*-Si:H band tail states (*cbt*). Spin-dependent tunneling to interface dangling bonds (*db*, *db′*) follows (solid arrow). Recombination is accomplished by spin-independent capture of a hole (broken arrow).

[see Fig. 2(a)]. The subsequent tunneling process into energetically lower lying dangling bond states *db* and *db′* is spin dependent because they are singly occupied. Since EDMR detects two *g* tensor orientations, it is obvious to assume that tunneling occurs via both configurations [Figs. 2(b) and 2(c)]. Once a dangling bond state is doubly occupied, spin-independent capture of a hole below the quasi-Fermi level E_{Fp} completes the recombination step.

In summary, by combining high-resolution EDMR measurements on real devices with state-of-the-art DFT calculations we were able to locate device-limiting paramagnetic states in a particular material phase and interface structure, assign their orbital configuration and extension into the Si tissue, and locate these states in the solar cell band structure. Observing spin-dependent recombination, we find evidence for the involvement of *a*-Si:H conduction band tail states and two different paramagnetic dangling bond states at the [111]-oriented buried *c*-Si surface. It is demonstrated that the *g* tensors of the localized *db* states are almost entirely dominated by the *c*-Si part of the junction and its roughness. Our work links the structure and function of the interface to the orbital symmetry of the recombination active defects. In particular, the important role of extended states in noncrystalline materials is shown. The isotropic *g* tensor of extended *a*-Si:H conduction band tail states is reproduced in quantitative agreement with the experiment, providing new insight into the long-standing debate about the character of the $g = 2.004(1)$ signal [41] in this kind of material. The present approach is of course not limited to *a*-Si:H/*c*-Si interfaces. It may as well be used to map paramagnetic states involved in spin-dependent transport in organic or other inorganic materials. It works for any degree of electronic (de)localization and may be extended to a large variety of electronically functional (hetero-)interfaces, thereby providing general insight into device limiting states and processes.

We are grateful to K. Jacob, C. Klimm and M. Muske (all HZB) for sample preparation and M. Schmidt (HZB) and C. Meier (FUB) for helpful discussions. The work was funded by the DFG (SPP 1601) and by the BMBF (EPR-Solar). The calculations have been performed at PC^2 (Paderborn) and HLRS (Stuttgart).

*alexander.schnegg@helmholtz-berlin.de
†uwe.gerstmann@uni-paderborn.de

[1] E. Yablonovitch, Science **246**, 347 (1989).
[2] H. J. Queisser, Science **281**, 945 (1998).
[3] H. Kroemer, ChemPhysChem **2**, 490 (2001).
[4] Y.-s. Huang, S. Westenhoff, I. Avilov, P. Sreearunothai, J. M. Hodgkiss, C. Deleener, R. H. Friend, and D. Beljonne, Nat. Mater. **7**, 483 (2008).
[5] R. A. McKee, F. J. Walker, and M. F. Chisholm, Science **293**, 468 (2001).
[6] R. Nicolini *et al.*, Phys. Rev. Lett. **72**, 294 (1994).
[7] A. Demkov and O. Sankey, Phys. Rev. Lett. **83**, 2038 (1999).
[8] M. Tanaka, M. Taguchi, T. Matsuyama, T. Sawada, S. Tsuda, S. Nakano, H. Hanafusa, and Y. Kuwano, Jpn. J. Appl. Phys. **31**, 3518 (1992).
[9] M. Tosolini, L. Colombo, and M. Peressi, Phys. Rev. B **69**, 075301 (2004).
[10] J. Gielis, P. van den Oever, B. Hoex, M. van de Sanden, and W. Kessels, Phys. Rev. B **77**, 205329 (2008).
[11] T. F. Schulze, L. Korte, F. Ruske, and B. Rech, Phys. Rev. B **83**, 165314 (2011).
[12] M. Sebastiani, L. Di Gaspare, G. Capellini, C. Bittencourt, and F. Evangelisti, Phys. Rev. Lett. **75**, 3352 (1995).
[13] S. Olibet, E. Vallat-Sauvain, and Ch. Ballif, Phys. Rev. B **76**, 035326 (2007).
[14] S. De Wolf, Ch. Ballif, and M. Kondo, Phys. Rev. B **85**, 113302 (2012).
[15] H. Matsuura, T. Okuno, H. Okushi, and K. Tanaka, J. Appl. Phys. **55**, 1012 (1984).
[16] T. F. Schulze, L. Korte, E. Conrad, M. Schmidt, and B. Rech, J. Appl. Phys. **107**, 023711 (2010).
[17] A. Schnegg, J. Behrends, M. Fehr, and K. Lips, Phys. Chem. Chem. Phys. **14**, 14 418 (2012).
[18] B. Langhanki, S. Greulich-Weber, J.-M. Spaeth, and J. Michel, Appl. Phys. Lett. **78**, 3633 (2001).
[19] A. Stesmans, Appl. Phys. Lett. **48**, 972 (1986).
[20] N. H. Thoan, M. Jivanescu, B. J. O'Sullivan, L. Pantisano, I. Gordon, V. V. Afanas'ev, and A. Stesmans, Appl. Phys. Lett. **100**, 142101 (2012).
[21] F. Hoehne, J. Lu, A. R. Stegner, M. Stutzmann, M. S. Brandt, M. Rohrmüller, W. G. Schmidt, and U. Gerstmann, Phys. Rev. Lett. **106**, 196101 (2011).

[22] T. Matsuoka, L. S. Vlasenko, M. P. Vlasenko, T. Sekiguchi, and K. M. Itoh, Appl. Phys. Lett. **100**, 152107 (2012).
[23] C. Pickard and F. Mauri, Phys. Rev. Lett. **88**, 086403 (2002).
[24] U. Gerstmann, M. Rohrmüller, F. Mauri, and W. G. Schmidt, Phys. Status Solidi C **7**, 157 (2010).
[25] M. Fehr *et al.*, Phys. Rev. B **84**, 245203 (2011).
[26] D. Ceresoli, U. Gerstmann, A. P. Seitsonen, and F. Mauri, Phys. Rev. B **81**, 060409R (2010).
[27] M. Schmidt, L. Korte, A. Laades, R. Stangl, Ch. Schubert, H. Angermann, E. Conrad, and K. v. Maydell, Thin Solid Films **515**, 7475 (2007).
[28] J. Behrends, A. Schnegg, M. Fehr, A. Lambertz, S. Haas, F. Finger, B. Rech, and K. Lips, Philos. Mag. **89**, 2655 (2009).
[29] See Supplemental Material at http://link.aps.org/supplemental/10.1103/PhysRevLett.110.136803 for EDMR raw data as well as details on experimental procedures and device simulations.
[30] P. J. Caplan, E. H. Poindexter, B. E. Deal, and R. R. Razouk, J. Appl. Phys. **50**, 5847 (1979).
[31] H. Angermann, W. Henrion, M. Rebien, and A. Röseler, Appl. Surf. Sci. **235**, 322 (2004).
[32] P. Giannozzi *et al.*, J. Phys. Condens. Matter **21**, 395502 (2009); http://www.quantum-espresso.org.
[33] J. P. Perdew, K. Burke, and M. Ernzerhof, Phys. Rev. Lett. **78**, 1396 (1997).
[34] T. F. Schulze, H. N. Beushausen, C. Leendertz, A. Dobrich, B. Rech, and L. Korte, Appl. Phys. Lett. **96**, 252102 (2010).
[35] M. Brandt and M. Stutzmann, Phys. Rev. B **43**, 5184 (1991).
[36] K. Lips, S. Schütte, and W. Fuhs, Philos. Mag. B **65**, 945 (1992).
[37] C. F. Young, E. H. Poindexter, G. J. Gerardi, W. L. Warren, and D. J. Keeble, Phys. Rev. B **55**, 16 245 (1997).
[38] R. Müller, P. Kanschat, K. Lips, and W. Fuhs, J. Non-Cryst. Solids **269**, 1124 (2000).
[39] C. Boehme, J. Behrends, K. v. Maydell, M. Schmidt, and K. Lips, J. Non-Cryst. Solids **352**, 1113 (2006).
[40] J. Behrends, K. Lips, and C. Boehme, Phys. Rev. B **80**, 045207 (2009).
[41] T. Umeda, S. Yamasaki, J. Isoya, A. Matsuda, and K. Tanaka, Phys. Rev. Lett. **77**, 4600 (1996).
[42] K. A. Johnson and N. W. Ashcroft, Phys. Rev. B **58**, 15 548 (1998).